Three-dimensional interface modelling with two-dimensional seismic data: the Alpine crust–mantle boundary

F. Waldhauser,* E. Kissling, J. Ansorge and St. Mueller

Institute of Geophysics, Swiss Federal Institute of Technology, ETH Hönggerberg, CH-8093 Zürich, Switzerland. E-mail: kissling@tomo.ig.erdw.ethz.ch

SUMMARY

We present a new approach to determine the 3-D topography and lateral continuity of seismic interfaces using 2-D-derived controlled-source seismic reflector data. The aim of the approach is to give the simplest possible structure consistent with all reflector data and error estimates. We define simplicity of seismic interfaces by the degree of interface continuity (i.e. shortest length of offsets) and by the degree of interface roughness (least surface roughness). The method is applied to structural information of the crust–mantle boundary (Moho) obtained from over 250 controlled-source seismic reflection and refraction profiles in the greater Alpine region. The reflected and refracted phases from the Moho interface and their interpretation regarding crustal thickness are reviewed and their reliability weighted. Weights assigned to each reflector element are transformed to depth errors considering Fresnel volumes. The 2-D-derived reflector elements are relocated in space (3-D migration) and interpolation is performed between the observed reflector elements to obtain continuity of model parameters. Interface offsets are introduced only where required according to the principle of simplicity.

The resulting 3-D model of the Alpine crust–mantle boundary shows two offsets that divide the interface into a European, an Adriatic and a Ligurian Moho, with the European Moho subducting below the Adriatic Moho, and with the Adriatic Moho underthrusting the Ligurian Moho. Each sub-interface depicts the smoothest possible (i.e. simplest) surface, fitting the reflector data within their assigned errors. The results are consistent with previous studies for those regions with dense and reliable controlled-source seismic data. The newly derived Alpine Moho interface, however, surpasses earlier studies by its lateral extent over an area of about 600 km by 600 km, by quantifying reliability estimates along the interface, and by obeying the principle of being consistently as simple as possible.

Key words: Alps, crustal structure, Moho reflection, seismic modelling, seismic resolution, topography.

1 INTRODUCTION

During the past 40 years, the greater Alpine region has been intensively probed by controlled-source seismology (CSS) methods (see Fig. 1) and a wealth of seismic data regarding the crustal structure and thickness have been accumulated. Refraction and reflection seismic techniques are particularly well suited to detect and image seismic interfaces that exhibit a significant velocity and/or impedance contrast, the prime example of which is the Moho discontinuity (crust–mantle boundary). The nearly universal observation of refracted (*Pn*)

and wide-angle reflected (*PmP*) waves from the crust–mantle boundary, and the general continuity of these phases along crustal seismic profiles, indicate that the Moho exists virtually everywhere beneath continents and is generally a continuous feature (Braile & Chiang 1986).

The great interest of Earth scientists in the depth, topography and lateral continuity of the Moho in orogenic belts, in particular, reflects the importance of this interface in crustal balancing, rheological and geodynamic modelling, to name just a few fields of study. In addition, the reflected and refracted Moho phases are easily identified in crustal seismic profiling and, therefore, serve as guides to identify less clear earlier and later phases in the record sections. Quantitative error estimates of Moho depths and topography are of great importance to any usage of this key horizon in crustal models.

* Now at: US Geological Survey, 345 Middlefield Rd, MS 977, Menlo Park, CA 94025, USA. E-mail: felix@andreas.wr.usgs.gov
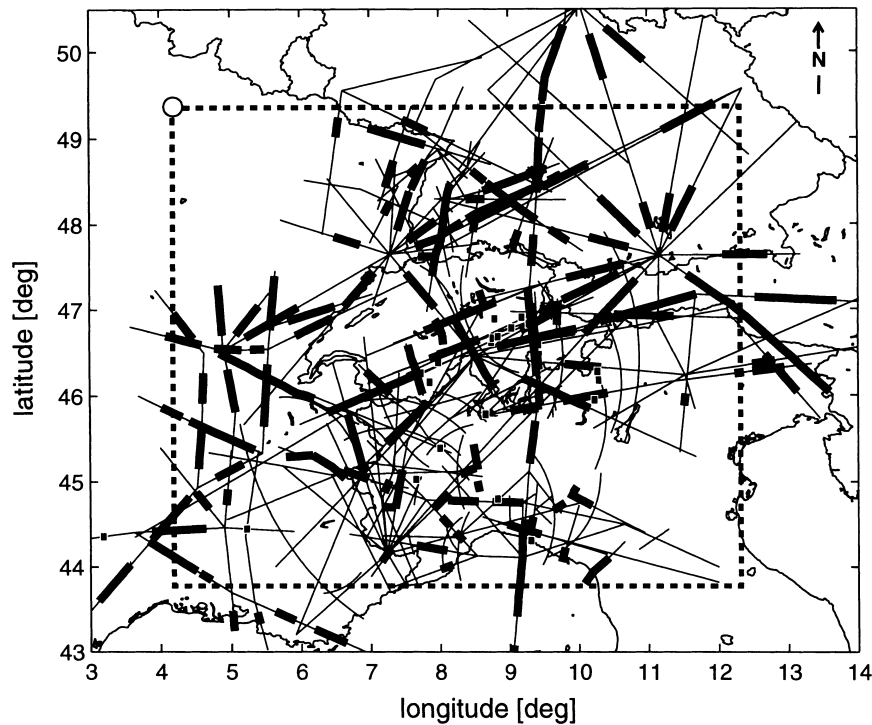
Figure 1. Seismic refraction/wide-angle reflection and near-vertical reflection profiles (thin lines) carried out over the past decades in the greater Alpine region. Superimposed are locations of 2-D-migrated Moho reflector elements (thick lines) taken from published interpretations of the controlled-source seismic profile data. The dashed box indicates the area for which the Moho interface is derived. The open circle at its NW corner facilitates orientation and comparison with Fig. 6.

Over the years, Alpine seismic data have been interpreted by various techniques such as 1-D Herglotz–Wiechert inversion, 2-D ray-tracing methods and synthetic seismogram modelling to estimate the location of seismic interfaces and associated velocities below the profile [see e.g. Egloff (1979) for 1-D interpretations, Aichroth, Prodehl & Thybo (1992) and Ye et al. (1995) for 2-D interpretations]. This information has usually been published as seismic cross-sections along profiles, with very few such models including even qualitative error estimates for derived structures (Kissling 1993). The seismic model information, however, shows large uncertainties, mainly as a result of different acquisition and interpretation techniques and the complex tectonic settings in the area of investigation. Since controlled-source seismic methods are basically 2-D techniques often applied to 3-D structures (in particular true for the Alpine orogen), CSS-derived reflector elements must be relocated in space (3-D migration). Before properly using the 2-D seismic model information for 3-D modelling, the reliability of the structural information contained in the published models needs to be assessed, weighted and expressed as spatial uncertainty of the reflector-element locations.

Based on 2-D seismic model information and appropriate error estimates, a procedure is developed that searches for simplest interfaces (Waldhauser 1996). Simplicity of seismic interfaces is defined by the degree of interface continuity and by the degree of interface roughness. The two most crucial steps in obtaining such simplest interfaces are 3-D migration and interpolation. While in-line migration of reflector elements is already performed by 2-D interpretations of CSS data, off-line location of these reflector elements, however, remains ambiguous. In the case of networked profiles, as in the Alpine

region, ambiguity can be partly overcome by using structural information from nearby cross-profiles (Kissling, Ansorge & Baumann 1997). Lateral continuity of an interface is achieved by interpolation between observed reflector data. The search for the smoothest interfaces with respect to error estimates for reflector elements requires an adequate interpolation algorithm suitable to control surface roughness. Based on the principle of interface simplicity, a minimal number and length of interface offsets are introduced.

The method developed for such 3-D interface modelling is applied to the seismic data from the Moho in the Alpine region to derive the smoothest and laterally most continuous interface (principle of simplicity) that accounts for all 3-D-migrated data within their estimated error bounds.

2 SEISMIC MOHO DATA AND ERROR ESTIMATES

2.1 Moho reflector elements

The controlled-source seismic (CSS) profile network in the greater Alpine region (Fig. 1) consists of over 200 reversed and unreversed wide-angle reflection and refraction profiles (in short, refraction profiles), 25 fan observations and 30 near-vertical reflection profiles (for overviews on the experimental activities see, e.g., Giese, Prodehl & Stein 1976; Roure, Heitzmann & Polino 1990; Meissner & Bortfeld 1990; Meissner et al. 1991; Freeman & Mueller 1992; Buness 1992 and references therein; Montrasio & Sciesa 1994; Prodehl, Mueller & Haak 1995; Ansorge & Baumann 1997; Pfiffner et al. 1997). The most striking feature in the CSS record sections are the

reflected phases from the Moho (*PmP*), which can be observed on almost every wide-angle reflection profile with lengths greater than about 100 km—depending on crustal thickness and average velocity—and many near-vertical reflection profiles, indicating that the Alpine Moho is generally a continuous feature. The *PmP* phases have been interpreted by 1-D and 2-D methods to determine crustal thickness. This structural Moho information has been systematically re-evaluated and compiled by locating the actually imaged reflecting structural element (in short, reflector element) below the profile (Fig. 1).

2.2 Reflector element weighting and depth errors

The compiled Moho reflector elements show a large range of uncertainty. Data quality increased over the years with smaller shot and receiver spacings, and identification and interpretation of reflected phases is becoming more reliable with modern 2-D ray-tracing techniques. Furthermore, complex 3-D tectonic settings with pronounced lateral variations strongly influence the reliability of the 2-D interpretation. In this study, the information quality of reflector elements is estimated using the weighting scheme proposed by Kissling (1993) and elaborated by Baumann (1994) with separate weighting criteria for wide-angle and near-vertical reflection surveys (see Table 1). Reflector elements derived from wide-angle profiles are weighted considering raw data quality (w_c) (confidence in correlation of phases), profile orientation relative to the 3-D tectonic setting (w_o) and profile type (reversed or unreversed profiles, fans) (w_t). Reflector elements from near-vertical reflection profiling are attributed with weights for quality of reflectivity signature (w_{cr}), type of migration (i.e. source of velocity used for migration) (w_{mig}) and projection distance (w_{proj}, projection of subsections on to one reflection profile). Total weighting factors (w_{tot}) were obtained by multiplying the individual weights:

$$w_{tot} = w_c w_o w_t \qquad \text{(refraction data),} \qquad (1)$$

$$w_{tot} = w_{cr} w_{mig} w_{proj} \qquad \text{(reflection data).} \qquad (2)$$

Total weighting factors between 0.1 and 1 are obtained for the structural Moho data in the Alpine region, with a large number of reflector elements having a factor of 0.6 (Fig. 2). Of course, although objectivity of the weighting scheme is strived for, the obtained weighting factors are still subjective.

By comparison with Fresnel-volume calculations for highest-quality data, the obtained total weighting factors are transformed into depth error estimates (Baumann 1994; Kissling *et al.* 1997). Considering an average frequency content of 6 Hz for Moho reflections from active sources and an average Alpine Moho depth of 40 km, and assuming perfect profile design and data ($w_{tot} = 1.0$), a vertical resolution $frsn_{err}$ of 3 km is
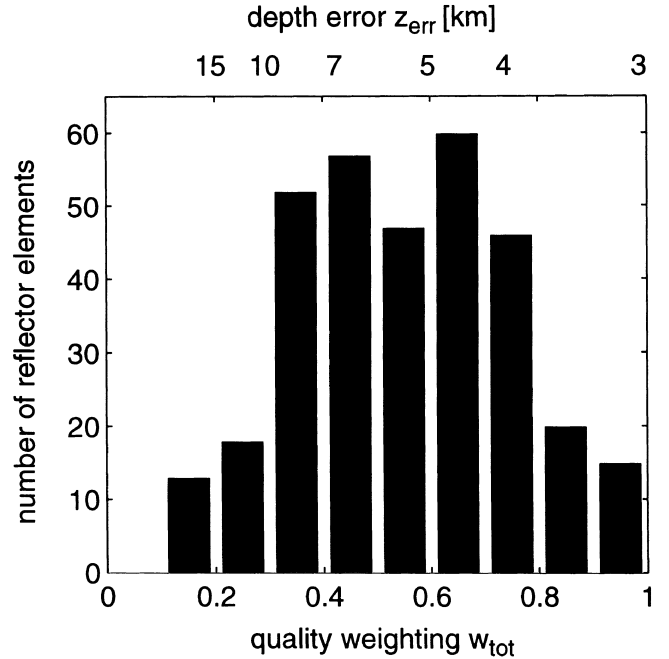

Figure 2. Distribution of weighting factors, w_{tot}, and depth error estimates, z_{err} in km, for Moho reflector elements derived from controlled-source seismic profiles. Weighting factors are transformed to depth scale using eq. (3).

Table 1. Weighting scheme for CSS-derived reflector elements (after Baumann 1994).

Wide-angle reflection and refraction profiles	Near-vertical reflection profiles:
Data quality, phase confidence (w_c)	*Reflectivity signature (w_{cr}):*
1.0 = Very confident	$1.0 - 0.2$ = Confidence rate of the reflectivity signature
0.8 = Confident	
0.6 = Likely	*Migration criteria (w_{mig}):*
0.4 = Poorly constrained	1.0 = Migration with independent velocities from refraction surveys
0.2 = Speculative	0.9 = Migration with stacking velocity from reflection profiles. Migration velocity model from refraction data projected over distances with no considerable structural changes
Profile orientation (w_c):	
1.0 = Along strike profiles; $0 \Leftarrow alpha \Leftarrow 10°$	
0.8 = Oblique profiles; $alpha > 10°$	0.8 = Else
Profile type, ray coverage (w_t):	*Projection criteria (w_{proj}):*
1.0 = Reversed refraction profile	1.0 = Projection distance <4 km
0.8 = Unreversed refraction profile	0.9 = Projection distance >4 km and <10 km
1.0 = Fan connected with reversed profile	0.8 = Projection distance >10 km
0.8 = Fan connected with unreversed profile	
0.6 = Unconnected fan	

derived. Based on this error estimate for the optimal case, the weight-dependent depth uncertainty (z_{err}) is estimated as

$$z_{err} = \frac{frsn_{err}}{w_{tot}} = \frac{\pm 3 \text{ km}}{w_{tot}}. \tag{3}$$

3 3-D SEISMIC INTERFACE MODELLING

3.1 Interface continuity and roughness

Specific criteria have to be assumed for the process by which the Moho topography is determined based on reflector-element locations and uncertainties. The simplest laterally continuous interface is sought, with vertical offsets only when required according to predefined criteria. We define the simplicity of a seismic interface by the degree of continuity and the degree of surface roughness of this interface.

Continuity along individual reflector elements is given by correlation of regularly observed phases reflected from the same element of a specific seismic interface. Correlation of seismic phases between profiles leads to the identification of reflector elements that belong to the same structural interface. Individual reflector elements, however, do not allow the prediction of continuity between them. In the case of the crust–mantle boundary, vertical discontinuity (offset) occurs when this seismic interface is interrupted by crustal-scale thrusting or crustal block faulting. In some cases, a vertical offset between reflector elements is revealed by discontinuously observed phases reflected from the same interface and along the same profile (e.g. Ye *et al.* 1995). Interface offsets can be assumed when ray-traced reflector elements or reflectivity patterns show an abrupt (relative to the general roughness) change in depth larger than their estimated depth errors. We quantify interface continuity by the length of interface offsets (i.e. shortest offset refers to highest continuity).

Interface roughness describes interface depth variations relative to a smooth reference interface and is a direct measure for the complexity of a continuous interface. We quantify interface roughness *rgh* by applying the 2-D finite-difference Laplacian operator to the regular surface grid:

$$rgh = \sum_{i=2}^{i_{max}-1} \sum_{j=2}^{j_{max}-1} \left(4z_{i,j} - z_{(i-1),j} - z_{i,(j+1)} - z_{(i+1),j} - z_{i,(j-1)}\right)^2, \tag{4}$$

where $z_{i,j}$ is the discrete depth value at grid node (i,j), and i_{max} and j_{max} are the maximal grid nodes in i and j directions, respectively. Equation (4), however, allows one to compare roughness values *rgh* only for interfaces with equal numbers of nodes.

Even a large set of sampled reflector elements does not allow unique prediction of interface depths. Hence, a broad range of interpolated interfaces differing in complexity of roughness and/or continuity is possible (see Fig. 3). Assuming a set of possible interfaces that fit all reflector elements within their uncertainties, one end of the spectrum is marked by an interface that has highest continuity, but, as a consequence, is most complex in its roughness (line A in Fig. 3). The high roughness value results from the attempt to interpolate between large vertical offsets of some reflector elements in order to obtain a spatially continuous interface. The other end of the spectrum marks an interface with numerous vertical offsets (line B in Fig. 3). In effect, this interface consists of several planes (sub-interfaces) that are discontinuous at those locations where the corresponding interpolated interface would lie outside the depth uncertainty. The objective here is to find the simplest interface (equally weighting continuity and roughness) featuring highest continuity (minimal number and length of offsets) and least roughness that fits all reflector elements within their error limits (line C in Fig. 3).

3.2 3-D migration

Controlled-source seismic methods are often 2-D techniques applied to 3-D structures such as the Alps and thus the compiled Moho reflector elements (Fig. 1) are not properly located in space. Migration is the process of restoring 3-D structures from 2-D CSS-derived reflecting structural elements (or reflectivity patterns). For the case of a homogeneous 2-D cylindrical structure (Kissling *et al.* 1997), reflector elements from transverse CSS profiles migrate in-line along the profile in the direction of the up-dipping interface (in-line migration). For along-strike profiles, reflector elements lie outside the vertical plane beneath the profile and migrate perpendicular to the profile (off-line migration).

In-line migration of reflector elements along the profile can be properly carried out by migration algorithms applied to near-vertical reflection data (e.g. Mayrand, Green & Milkereit
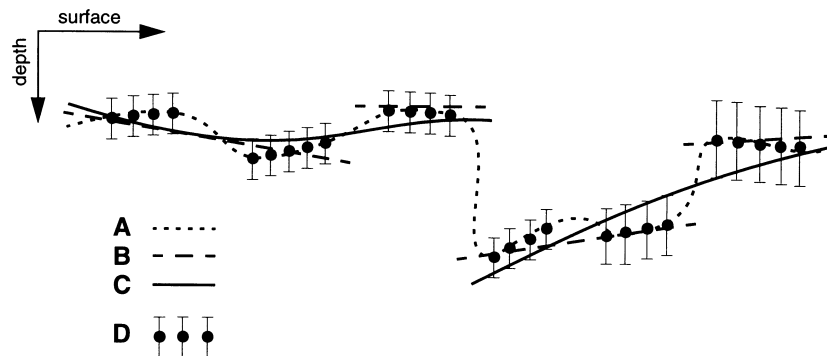

Figure 3. Types of possible interpolated interfaces (A, B and C) with varying roughness/continuity to interpolate reflector elements (D) represented by structural depth points within their uncertainty (error bar at each structural depth point). A: Rough interface with exact data point fit. B: Straight-line interfaces that exhibit several vertical offsets (roughness zero for an individual sub-interface). C: Smooth interface that accounts for data uncertainty and shows vertical offsets when required according to the principle of interface simplicity.

1987; Holliger & Kissling 1991) or by 2-D ray-tracing methods applied to wide-angle reflection data (e.g. Ye *et al.* 1995). 1-D interpretation methods generally project reflector depths to locations below the shot point (e.g. Egloff 1979). In the scope of this work, and in areas of laterally homogeneous structures only, such 1-D-derived reflector elements have been approximately migrated in-line to half the distance of the phase observations.

None of the above-mentioned methods provides off-line migration of the structures along individual profiles. In the case of networked profiles, the inherent ambiguity can be overcome by using additional structural information from nearby profiles. Off-line migration of reflector elements from longitudinal profiles can be verified by in-line migrated reflector elements from transverse crossing profiles (Ye *et al.* 1995). Off-line migration of reflector elements from oblique crossing profiles cannot be determined exactly, since the migration vector cannot be correctly separated into in-line and off-line components.

The case of a CSS network with perpendicular crossing along-strike and transverse profiles to determine accurately off-line migration of in-line migrated along-strike structures is rare. More often we have to deal with loosely networked CSS profiles as in the Alpine region. For the migration process on the Alpine data, we separate the 3-D migration vector for all reflector elements into in-line and off-line components (see Fig. 4). In the case of reflector elements derived from oblique profiles, the so-derived 3-D migration is an approximation to the real 3-D migration. Owing to the smaller weight given to oblique profiles (see Table 1), the lateral and vertical migration errors for these profiles will, therefore, be in the range of the depth uncertainty of the corresponding reflector elements.
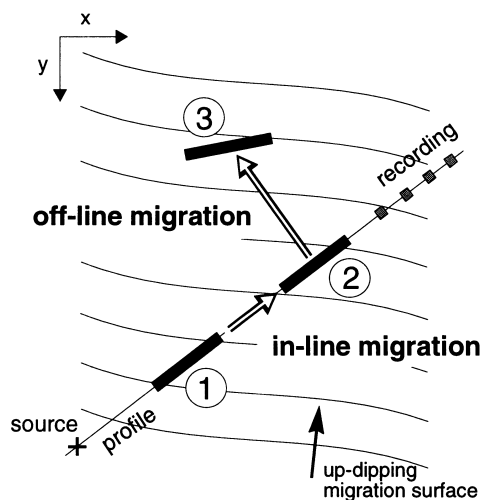

Figure 4. Map view of the 3-D migration procedure. Separation of 3-D migration vector into an in-line $(1 \rightarrow 2)$ and off-line $(2 \rightarrow 3)$ component. An unmigrated reflector element (1) has been in-line migrated by means of 2-D ray tracing. The in-line migrated reflector element (2) is off-line migrated perpendicular to the profile in the direction of updipping migration surface represented by depth isolines, producing the 3-D-migrated reflector element (3). The position of the 3-D-migrated reflector element is found by searching for ray paths with perpendicular incidence on the 3-D-migration surface. The migration surface in the vicinity of the element to be migrated is obtained by initial interpolation of reflectors belonging to the same interface.

Migration of CSS-derived reflector elements is based on the general trend of the imaged interface (migration surface) in the vicinity of the reflector element. The 3-D-migration surface is obtained by an initial interpolation between the in-line migrated CSS-derived reflector elements (e.g. Fig. 1). 2-D-interpreted and, therefore, properly in-line migrated reflector elements are off-line migrated perpendicular to the profile in the up-dipping direction of the initial 3-D-migration surface (see Fig. 4). 1-D-interpreted and approximately in-line migrated reflector elements are also migrated in the direction of the up-dipping 3-D-migration surface. The location of the 3-D-migrated reflector element is found by searching for the ray path with incidence perpendicular to the 3-D-migration surface. The velocity in the model is assumed to be constant (ray-theoretical migration) and, therefore, effects from intra-crustal velocity inhomogeneities on the 3-D-migration path are neglected.

This 3-D-migration process can be successfully applied to smooth interfaces such as most parts of the Moho. In the vicinity of each reflector element, the interface can then be considered as plane and the separation of the migration path is reasonable. Rough surfaces lead to migration path scattering and the method applied will not be able to perform such 3-D migration properly.

3.3 Interpolation

For the purpose of interpolation, reflector elements are discretized by a number of structural depth points sampled every 2 to 4 km along the individual profiles, depending on the factor with which the reflector elements are weighted. Higher weights imply higher density of structural depth points along reflector elements. A two-step procedure is applied in each interpolation process (Klingelé 1972). In a first step, Moho depths are calculated for a coarse regular grid with a grid spacing of 18 km appropriate for the distribution and density of the observed Moho reflector elements (Fig. 1). This interpolation is carried out by least-squares fitting of polynomial surfaces (see e.g. Lancaster & Salkauskas 1986). Local parabolas, described by second-order polynomials, are computed with their apices at the grid nodes to be interpolated. Data points within a predefined radius are approximated in a least-squares procedure, weighting each data point by the inverse of the distance to the centre of the circle.

The second step includes a refining of the initial grid to a spacing of 6 km, a value similar to the estimated average horizontal resolution obtained from CSS methods for the Moho interface. It is performed by a line-by-line interpolation followed by a column-by-column interpolation on the previously obtained grid, using a spline under tension whose variations of the stress factor allow an interpolation ranging from broken line to a classical bi-cubic spline (Cline 1974).

3.4 Procedure to derive the 3-D-migrated simplest Moho interface

The derivation of the simplest Moho interface accounting for all 3-D-migrated data within their error limits consists of seven steps (see Fig. 5).

Step 1 Interpolation of 2-D-migrated and discretized Moho reflector elements (i.e. structural depth points) for single (=highest-continuity) interfaces of variable roughness.
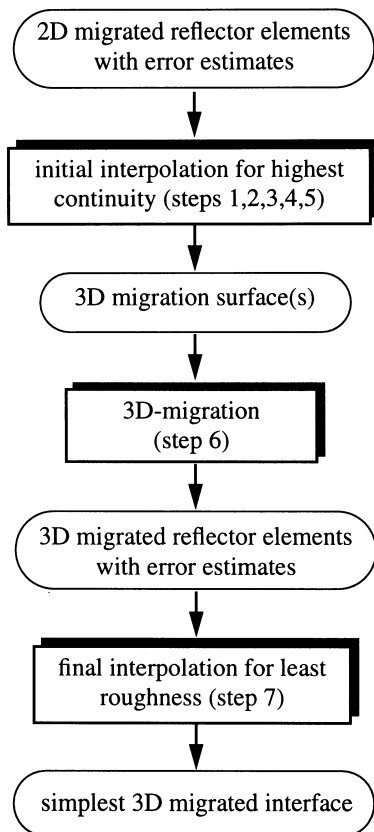
characterized by equally high continuity and differ only in their roughness. Fig. 6 gives a perspective view of four such interfaces, M_{55} ($rgh = 55$, very smooth), M_{201}, M_{588} and M_{4993} (extremely rough), representing selected roughness values.

4.2 Step 2: best-fitting single interface

The quality of each interpolation, based on the variance of the misfit relative to the observation errors, and on the physical principle of interface continuity, is quantified by the root-mean-square (rms) value of the depth residuals for each interface individually:

$$z_{\text{rms}}^{\text{res}} = \sqrt{\dfrac{\sum\limits_{k=1}^{k_{\max}} (\Delta z_k)^2}{k_{\max}}}, \tag{5}$$

where Δz_k is the difference between observed and calculated depths of the kth reflector element, and $k_{\max}$ is the number of reflector elements used for interpolation.

Fig. 7 shows depth rms residuals for 14 of the 20 calculated surfaces between a roughness of 0 (plane) and 588 (rough). Solid circles indicate the three surfaces depicted in Fig. 6. Rms residuals decrease strongly from 10 km to about 3 km for increasingly rougher surfaces between $rgh = 0$ (plane) and about $rgh = 201$. Beyond a surface roughness of 201, rms residuals continue to decrease but only slowly to a value of about 2.4 km for a roughness of 588.

A 'best-fitting' single interface from the 20 calculated surfaces can be attached to the smallest reasonable error of ± 3 km (dashed line in Fig. 7), as defined previously by the optimal resolution capability of CSS methods. Interfaces with $rgh > 201$ show rms residuals smaller than the optimal depth error (Fig. 2), and thus tend to overfit the data. These interfaces represent unjustified rough Moho topography (see e.g. M_{588} or M_{4993} in Fig. 6). Rms residuals increase rapidly for smoother surfaces with depth misfits larger than the observed typical depth error. Thus, best-fitting interpolation is achieved with roughness around 201.

4.3 Step 3: continuous or discontinuous Moho interface

Fig. 8 shows the best-fitting single interface M_{201} by depth contours for a zoomed area encompassing the central and western Alps and northern Apennines. All structural depth points on the in-line migrated reflector elements (see Fig. 1) are used for this interpolation and are marked for the zoomed area by small grey dots in Fig. 8. No off-line migration is applied so far. In addition, structural depth points with a misfit to the selected interface M_{201} larger than the individual depth errors (significant depth misfits) are shown. Significant depth misfits systematically above the M_{201} surface are represented by large solid circles, and those located below the M_{201} surface by open circles. No significant depth misfits are observed outside the area shown in Fig. 8 within the greater Alpine area. The significant depth misfits remain also after 3-D migration of the 2-D-migrated reflector elements, despite the smoothing effect of the migration process.
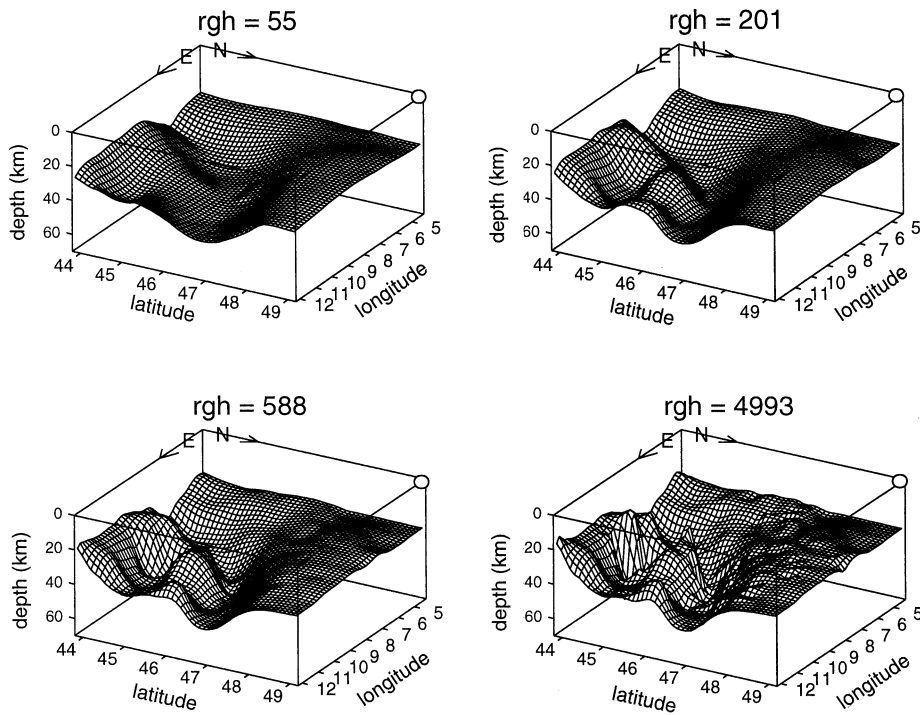

Figure 5. Process flow for 3-D interface modelling. See text for details and description of steps 1 to 7.

Step 2 Selection of the best-fitting single interface with appropriate roughness value (see below).

Step 3 Decision for continuous or discontinuous Moho interface.

Step 4 Introduction of the least number of necessary interface offsets (i.e. separation of interfaces) based on significant misfits between observed and calculated Moho depths (see below).

Step 5 Interpolation for 3-D-migration surface(s) using the least number of necessary offsets defined by step 4 and using for each surface the lowest roughness value fitting all 2-D-migrated data within their error limits.

Step 6 3-D migration of all observed Moho reflector elements based on individual 3-D-migration surface(s).

Step 7 Final interpolation of 3-D-migrated and discretized Moho reflector elements from step 6 using offsets defined by step 4 (i.e. number of separated interfaces) and using for each interface the lowest roughness value fitting all data within their error limits.

In the following, this procedure is applied to the crust–mantle boundary in the greater Alpine region.

4 THE ALPINE CRUST–MANTLE BOUNDARY

4.1 Step 1: single-interface interpolation

A set of 20 continuous interfaces $f_{1-20}(x, y)$ are interpolated using all 165 discretized Moho reflector elements within the Alpine region (see Fig. 1). These single interfaces are all

Figure 6. Perspective SW view of four continuous single surfaces representing the Alpine Moho with selected roughness values *rgh* within the range used for the initial interpolation process: M_{55}, M_{201}, M_{588} and M_{4993} surfaces.
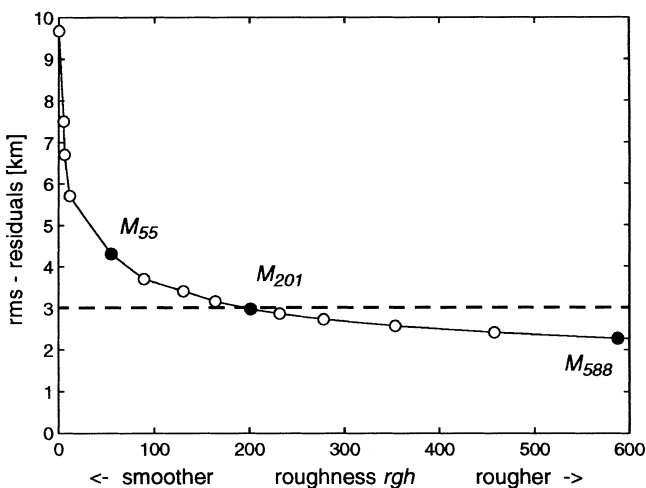

Figure 7. Depth rms residuals (km) for a set of single surfaces with roughness *rgh* between 0 (plane) and 588 (very rough). The dashed line represents depth uncertainty for the optimal case. Solid circles indicate surfaces depicted in Fig. 6.

4.4 Step 4: introduction of interface offsets

To avoid significant depth misfit, interface offsets have to be introduced in areas such as the south-central Alps (A in Fig. 8), the northern part of the western Alps (B) and the northern Apennines (C and D). Before doing so, it must be shown that the locations of these areas (A, B, C, D in Fig. 8) do not depend strongly on the chosen surface roughness (e.g. *rgh* = 201). Fig. 9 shows absolute depth residuals for the M_{201} surface and for surfaces with roughness 354 (rougher) and 89 (smoother).

A, B, C and D label significant depth misfits that occur in the corresponding areas indicated in Fig. 8. The rougher M_{354} surface (Fig. 9a) still shows considerable and significant depth misfits in the south-central Alps (A) and the northern Apennines (C), where evidence for Moho offsets is given by seismic wide-angle data along the European Geotraverse (EGT) (Ye *et al.* 1995). Smoothing the surface to a roughness of 89 (Fig. 9c) yields increased significant depth misfits at the same location as observed on the M_{201} surface. The comparison shows that the best-fitting single interface M_{201} outlines stable localities (A, B, C, D) of significant misfit, which must represent tectonic features. At these localities, the M_{201} interface is too smooth to follow the observed depths of the structural depth points within their error limits. The corresponding reflector elements lie systematically outside the interpolated interface and indicate interface offsets. Clusters of reflector elements with opposite-sign significant misfits are separated into two 'sub-interfaces' (see Fig. 10).

In area A (Figs 8 and 10) the European/Adriatic Moho transition is characterized by the south-dipping European Moho and the shallower, north-dipping Adriatic Moho. These dominant E–W-trending structural features are revealed by seismic data along the transverse near-vertical reflection profiles CT and ET (Fig. 8) (Holliger & Kissling 1991; Valasek & Mueller 1997) and along the refraction/wide-angle reflection profiles on the EGT (Ye *et al.* 1995). On the basis of depth error estimates for the imaged reflector elements, Baumann (1994) showed clear evidence for an offset between the two oppositely down-dipping Moho discontinuities. Thus, a WSW–ENE-striking Moho offset (bold line S_1 in Fig. 8) is introduced for area A_1 that separates the European Moho from the Adriatic Moho by about 15 km (Fig. 10).
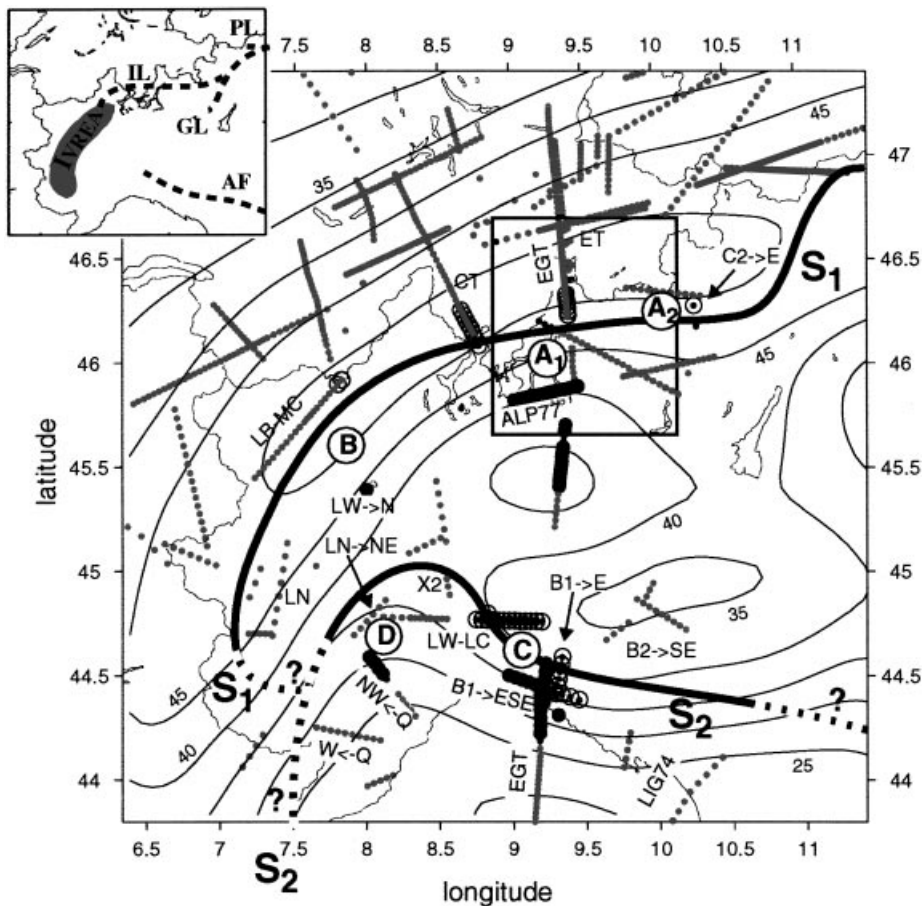
Figure 8. M$_{201}$ single surface Moho (contoured at 5-km intervals) derived by interpolation of all in-line migrated and discretized reflector elements (grey dots), yielding a depth rms residual of 3 km. Significant depth misfits of points lying above (filled circles) and below (open circles) the M$_{201}$ surface are shown. Proposed Moho offsets S$_1$ and S$_2$ are shown by bold continuous and dashed lines. Labels (e.g. LW-LC) identify CSS profiles. Figure inset shows major tectonic structures for the zoomed area (IL: Insubric Line; GL: Giudicarie Line; PL: Pustertal Line; AF: Apenninic Front). Box indicates area shown in Fig. 10. For labels A, B, C and D see text.

In area C a WNW–ESE-striking offset (bold line S$_2$ in Fig. 8) separates the south-dipping Adriatic Moho, disappearing beneath the Apennine front, from the shallower and slightly north-dipping Ligurian Moho. This offset is well documented by refraction profiles along the EGT (Egger 1992; Ye *et al.* 1995) and along the strike of the Apennines (LW ↔ LC, B1 → ESE; Buness 1992; Waldhauser 1996), and fan recordings from shotpoints B1 and B2 to the east (B1 → E, B2 → SE; Buness 1992).

As discussed above, interface offsets are first introduced in areas A$_1$ and C based solely on seismic information. This separation in both cases occurs near well-known suture zones encompassing the Adriatic crustal block. Hence, the separation into two interfaces is laterally continued into region B, where seismic data are not conclusive to obtain a precise location of offset relative to these tectonic elements (the Periadriatic tectonic Lineament; Laubscher 1983) nor to obtain the dip of the specific reflector elements. By following the Insubric Line (IL, see Fig. 8, inset) (Schmid, Zingg & Handy 1987) along the strike of the ESE-dipping western Alpine Moho (Thouvenot *et al.* 1990; Sénéchal & Thouvenot 1991; Kissling 1993), offset S$_1$ forms an arc between the European and the Adriatic Moho from location A$_1$ in the WSW direction (Fig. 8). Evidence for a vertical continuation of this suture line with

depth is given by the significant depth misfits observed along the refraction profile LB ↔ MC (Moho depth of about 55 km; Ansorge 1968) and the fan profile LW → N (Moho depth of about 25 km; Thouvenot *et al.* 1990) (see area B in Fig. 8). The proposed course of S$_1$ between the significant depth misfits in area B is guided by the Ivrea body, an intracrustal high-density and high-velocity structure with clear association to the Adriatic crust (Schmid *et al.* 1987; Solarino *et al.* 1997). According to the spatial extension of this dominant structure (Solarino *et al.* 1997), offset S$_1$ runs along its western margin to the south, separating the deep European Moho from the shallow, southeast-dipping Adriatic Moho and the associated high-velocity Ivrea body. No seismic data, however, show direct evidence for continuity between the Adriatic Moho and the high velocities of the Ivrea body (Solarino *et al.* 1997). The south-dipping group of reflector elements (labelled LN in Fig. 8; see Ansorge 1968) south of area B is, therefore, associated with the Adriatic Moho featuring similar dip for this area. The exact location of S$_1$ south of the Ivrea body, i.e. the transition between the Adriatic and European Moho in this area, is not revealed by seismic data and is represented by the shortest offset length possible (dashed part of S$_1$), joining the Ligurian Moho (see below) at about 44.4° latitude and 7.6° longitude.
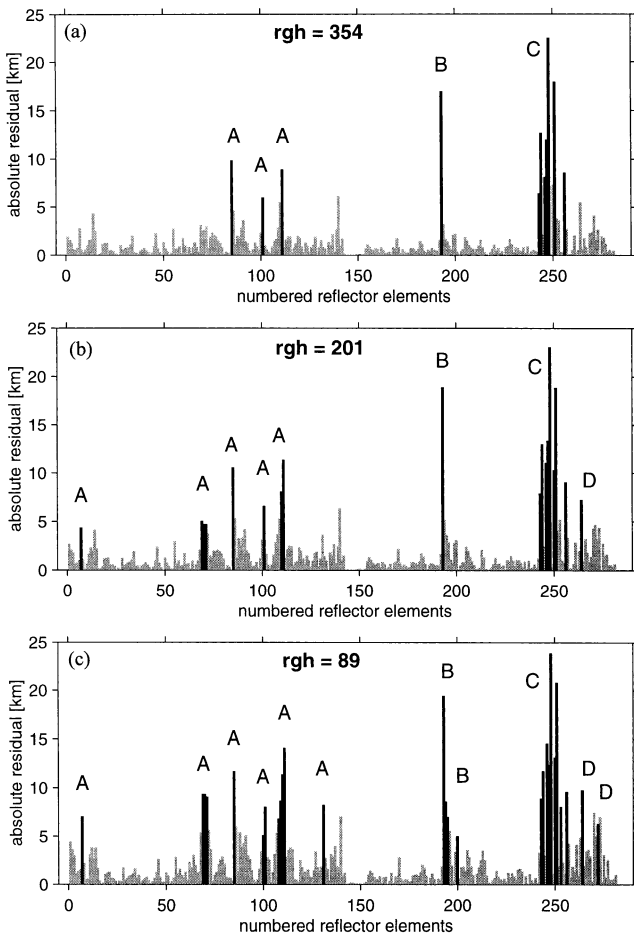
Figure 9. Absolute depth residuals for single surfaces (a) M_{354}, (b) M_{201} and (c) M_{89}. Black bars A, B, C and D indicate areas (see Fig. 8) where significant depth misfits are observed.

From location A_1 (Fig. 8) to the east, only a fan profile ($C2 \rightarrow E$, see area A_2 in Fig. 8) indicates a south-dipping European Moho and a slightly shallower, north-dipping Adriatic Moho (Musacchio *et al.* 1993). The distinct significant depth misfit in area A_2 is at least partly caused by 3-D-migration effects. Whether the transition from the European to the Adriatic Moho is a trough or consists of one or several small offsets is not revealed by the available data. Still in accordance with the little seismic information available (see also Fig. 1), the further continuation of S_1 to the eastern limits of our model follows the Periadriatic Lineament (Laubscher 1983), i.e. along the Insubric Line (IL), the NNE-wards trending Giudicarie Line (GL), and along the ESE-wards running Pustertal Line (PL) (see Fig. 8, inset).

The Moho offset S_2 at location C (Fig. 8) is traced to the northwest, and merges into a south-turning arc encircling the shallow reflector elements determined from refraction profiles $LW \leftrightarrow LC$, $Q \rightarrow NW$, $Q \rightarrow W$ (Buness 1992) and $LN \rightarrow NE$ (Stein, Vecchia & Froelich 1978), and from the fan profile X2 (Nadir 1988), which belong to the Ligurian Moho (location D). A 3-D interpretation of the $LW \leftrightarrow LC$ profile (Waldhauser *et al.* 1994) migrates the reflector element of the Ligurian Moho to the south and that of the Adriatic Moho to the north, and clearly indicates that the Moho offset modelled at

location C extends to the northwest below the $LW \leftrightarrow LC$ profile (location D). Such an offset improves the fit with the structural data at location D. The exact position of the triple junction where the European, the Adriatic and the Ligurian Moho join, however, is not revealed by the seismic data available. Also the southward continuation of offset S_2 (i.e. the transition between the European and the Ligurian Moho) remains uncertain (dashed part of S_2).

East of area C (Fig. 8), seismic data from refraction profile $B2 \rightarrow SE$ and from fan observation $B2 \rightarrow SW$ indicate a still south-dipping Adriatic Moho (Buness 1992), most likely separated from the Ligurian Moho, which continues at shallow depth (LIG74 refraction profiles; Colombi, Guerra & Scarascia 1977; Buness 1992). This is consistent with the course of the Apenninic Front (AF, see Fig. 8, inset) observed at the surface, along which offset S_2 is traced to the eastern limit of the model.

4.5 Step 5: interpolation for three migration surfaces

Three surfaces are obtained by opening the single interface M_{201} along S_1 and S_2 (see Fig. 8), i.e. separating the reflector elements along these lines and performing individual interpolation of the European (north of S_1), Adriatic (between S_1 and S_2) and Ligurian (south of S_2) Moho data. Fig. 10 illustrates the effect of opening the single interface between the observed significant depth misfits using the Moho in the south-central Alps as an example (see box in Fig. 8 for location). Fig. 10(a) shows in an ESE-oriented perspective view the single M_{201} surface with unmigrated structural depth points and their error bars along reflector elements. Significant depth misfits are indicated by arrows on the surface. Fig. 10(b) shows the European (north) and Adriatic (south) Moho after opening the single M_{201} surface along S_1 and after individual interpolation.

Numerical instabilities during interpolation at the surface edges are avoided by using auxiliary depth points outside the surfaces where necessary, linearly extrapolating the geometry of the area near the interface edge. In areas of few (e.g. NE Po Plain; Slejko *et al.* 1987), unreliable or even no seismic data within the model frame, such as in the northwestern part (eastern France), auxiliary depth points are used for interpolation that produce the simplest Moho topography consistent with gravity data. For example, Moho depths based on the Verona gravity high are taken into account for the eastern Po Plain area.

Again, a set of 20 surfaces featuring a broad roughness range is calculated for each of the three Mohos separately. Smoothest surfaces (migration surfaces) are sought that fit all data within observed depth errors, i.e. without significant depth misfit. In Fig. 11, the number of significant depth misfits is plotted against surface roughness for each migration surface. Roughness values are chosen for the European ($rgh = 13.8$), the Adriatic ($rgh = 52.6$) and the Ligurian ($rgh = 1.9$) migration surfaces (Figs 11a, b and c, respectively).

4.6 Step 6: 3-D migration

To complete 3-D migration, off-line migration of the 2-D in-line migrated reflector elements along the migration surfaces M_{14}^{eur}, M_{53}^{adr} and M_{2}^{lig} (Fig. 12) is subsequently performed using the method described in Section 3.2 (see also Fig. 4). Consistent migration vector orientations are obtained, with a maximum horizontal displacement of about 17 km (Fig. 12). More than
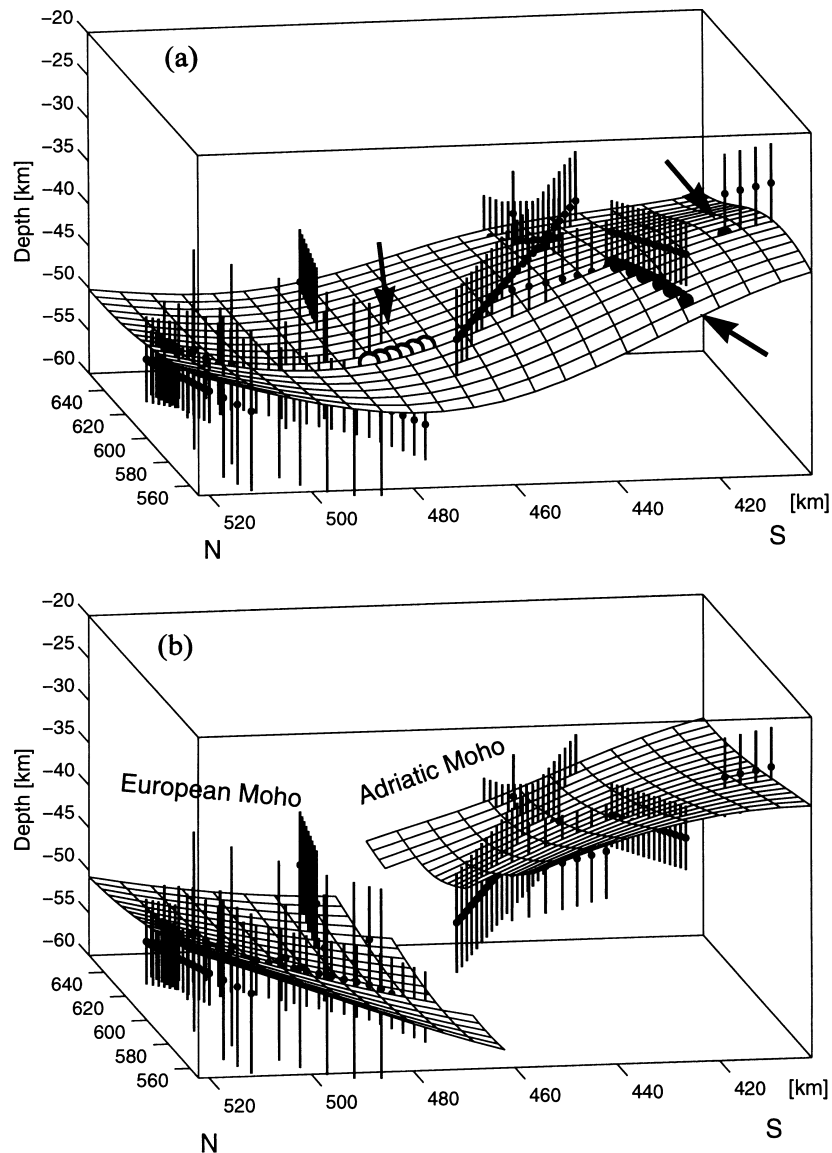
Figure 10. (a) Perspective ESE-oriented view on continuous M_{201} surface of the Moho in the region of the south-central Alps below the Insubric Line along the EGT (see box in Fig. 8). Arrows indicate structural depth points with depth errors and significant depth misfits on the M_{201} surface. (b) Same perspective view on the Moho offset between European Moho (N) and Adriatic Moho (S) after opening the M_{201} surface along S_1 in Fig. 8.

2 km for the vertical component of migration vectors in the northern Apennines is obtained, where the deep-reaching and strongly dipping Adriatic Moho is mainly imaged by along-strike profiles. Reflector elements from the European Moho along the Alpine longitudinal profiles migrate by about 1 km in the vertical direction.

4.7 Step 7: final interpolation for three sub-interfaces

The 3-D-migrated reflector elements are used in a final interpolation process, again selecting the three smoothest Moho sub-interfaces that still fit the European, the Adriatic and the Liguarian reflector data within the error limits, and including the required interface offsets according to the principle of simplicity (Fig. 13).

5 DISCUSSION AND CONCLUSIONS

The resulting model of the Alpine Moho (Fig. 13) shows two offsets with three sub-interfaces: the European, the Adriatic and the Ligurian Moho. Moho depths are in good accord with previous studies for those regions with dense and reliable controlled-source data (Ansorge *et al.* 1987; Nadir 1988; Valasek 1992; Giese & Buness 1992; Kissling 1993; Baumann 1994; Hitz 1995), and with recent studies using local earthquake data (Solarino *et al.* 1997; Parolai, Spallarossa & Eva 1997). The Alpine Moho interface derived in this study surpasses earlier studies by its lateral extent over an area of about 600 km by 600 km, by quantifying reliability estimates along the interface (see Fig. 13) and by obeying the principle of being consistently as simple as possible.
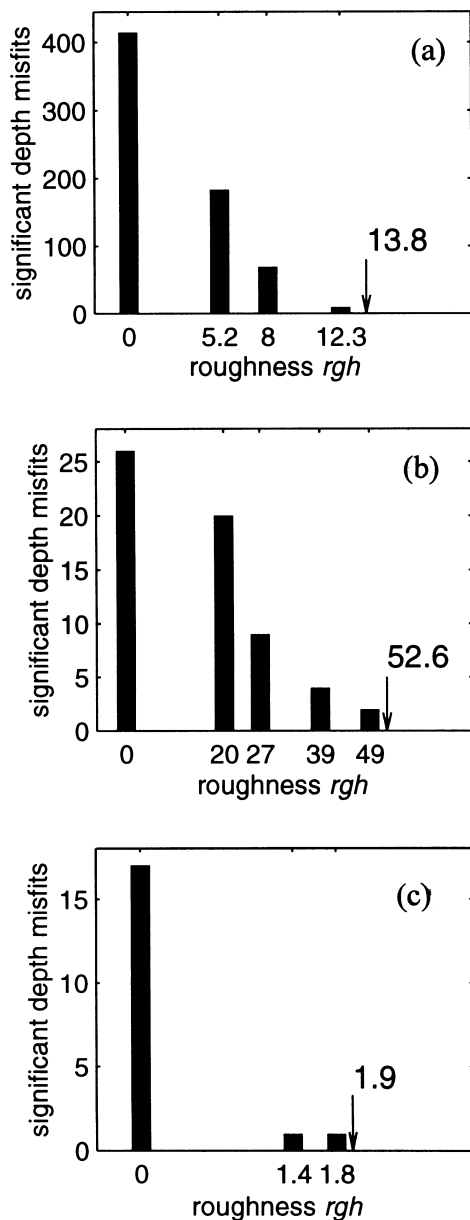
Figure 11. Number of significant depth misfits as a function of surface roughness *rgh* for (a) European, (b) Adriatic and (c) Ligurian migration surfaces.

Below the central Alps the European Moho (Fig. 13) features a south-dipping interface, deepening from 28 km below the stable foreland to more than 55 km below the Insubric Line. This structure is well constrained by combined wide-angle and near-vertical reflection data. A further southward continuation of the European Moho below the Adriatic Moho, as, for example, proposed by Valasek (1992), has not been reliably imaged by controlled-source seismic methods but seems plausible in the light of tectonic models (Schmid *et al.* 1996). The European Moho below the central Alps changes to the east-dipping arc of the western Alps. The shape of the European Moho below the southern end of the western Alps cannot be determined reliably because of missing seismic data (see also Fig. 1). The proposed offset between the European and Ligurian Moho (see also S$_2$ to the west in Fig. 8) is less reliable.

The Adriatic Moho (Fig. 13) is best imaged along the EGT profile, where it is updoming below the Po Plain between the European and the Ligurian Moho. At the northern rim, the Adriatic Moho is underthrusted by the European Moho, whereas at the southern rim it is overthrusted by the Ligurian crustal block. The southern Adriatic Moho is lost at a depth of about 54 km and a further deepening cannot be determined by available 2-D controlled-source seismic methods. Further to the west, near the western margin of the Po Plain, the Adriatic Moho merges into the structure of the Ivrea zone (see Fig. 13b), where the situation again remains unclear. Strong near-surface reflections related to the Ivrea body, with phase characteristics of *PmP* phases, can be observed in this region (Berckhemer 1968). No seismic evidence exists for a direct contact between these near-surface reflections attributed to the high-velocity Ivrea body and the *PmP* reflections from the Adriatic Moho further east. The Ivrea body with its Moho-like velocity contrast is considered, however, as an intracrustal high-velocity zone (Solarino *et al.* 1997) associated with the Adriatic Moho. A direct contact between the Adriatic and European Moho may possibly exist below the southwestern Po Plain, where the two Mohos show a similar depth of about 48 km. The updoming eastern part of the Adriatic Moho, where no seismic data are available (see also Fig. 1), has tentatively been modelled by eastward extrapolation of the observed structure in the central part in accordance with observed gravity data (Slejko *et al.* 1987; Carozzo *et al.* 1991).

The Ligurian Moho (Fig. 13) along the EGT beneath the Apennines is well located at a shallow depth of around 20 km. At its northern rim, below the front of the Apennines, the Ligurian Moho shows an offset of about 30 km relative to the deeper Adriatic Moho. West of the EGT profile, the Ligurian Moho shows possibly a slight deepening, ending below the western Po Plain. There the Ligurian Moho lies above the European Moho, separated by an offset of about 10 km. To the east of the EGT profile, the Ligurian Moho seems to continue in a shallow fashion, with unrevealed contact to the Adriatic Moho.

The obtained Alpine Moho topography reflects the present large-scale Alpine tectonic structure resulting from the collision of the African Plate with the European Plate. The two Moho offsets below the Insubric Line and below the northern Apennines confirm a southward subduction of the European Moho under the shallower, north-dipping Adriatic Moho, and a southward subduction of the Adriatic Moho beneath the Ligurian Moho. The Adriatic Moho is updoming below the Po Plain (see Fig. 13), most likely as the combined result of compressional forces due to the NNW-drifting African Plate and of subduction-related loading beneath the northern Apennines.

None of the presently available CSS data provide conclusive and direct evidence that the European and the Adriatic lithosphere penetrate deep into the upper mantle beneath the southern Alps and the Liguarian Sea, respectively. Crustal balancing considerations (Pfiffner *et al.* 1990; Ménard, Molnar & Platt 1991), however, suggest a continuation also of lower European crust beneath the Adriatic upper mantle south of the Insubric Line (Schmid *et al.* 1996). Such a subduction structure is also likely below the Apennines, where the Adriatic Moho underthrusts the Ligurian Moho. To resolve lithospheric slab structures beneath an overriding plate, however, requires deep-seated seismic sources as are employed by local
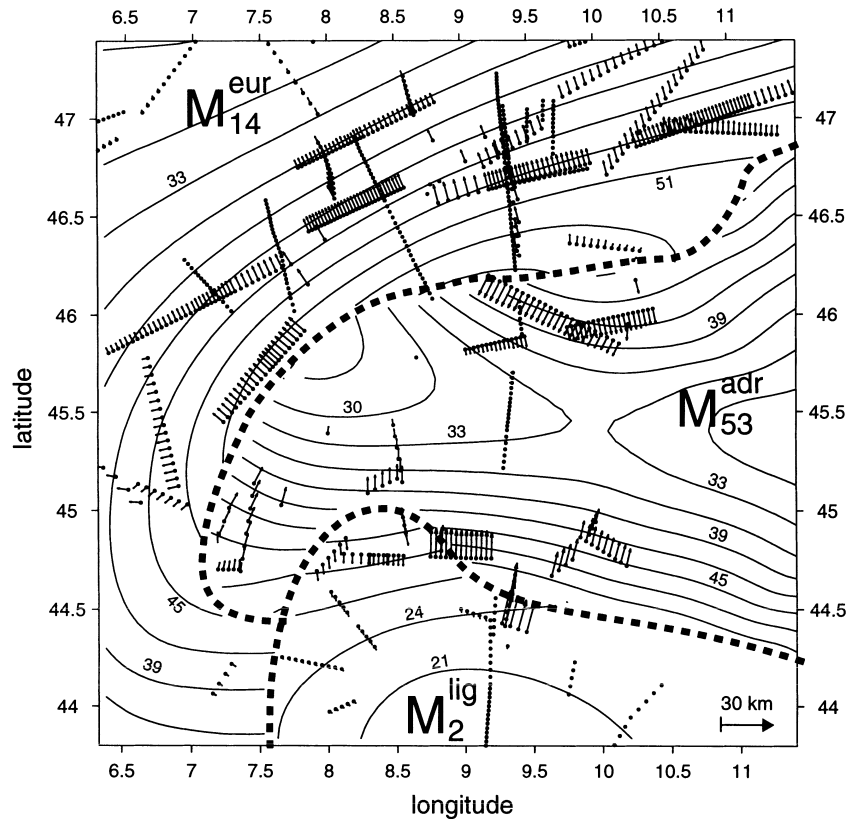
Figure 12. Migration surfaces for the European Moho (*rgh* = 14), the Adriatic Moho (*rgh* = 53) and the Ligurian Moho (*rgh* = 2) represented by depth isolines at 3-km intervals for area as in Fig. 8. Isoline values are indicated by numbers. Horizontal components of the 3-D migration vectors are marked by arrows. For migration distance in km, see reference arrow in lower right corner.

earthquake and teleseismic tomography (e.g. Spakman, Van der Lee & Van der Hilst 1993; Solarino *et al.* 1997).

In contrast to previous studies to derive a map of Moho topography (e.g. Buness 1992; Scarascia & Cassinis 1997), the new technique presented in this paper aims to find the simplest possible interface that is consistent with all 3-D-migrated CSS data within their previously specified error estimates. A fundamentally different approach has, for example, been taken by Giese & Buness (1992) and Scarascia & Cassinis (1997), who obtained rather complex Moho structures with several offsets and fragmentations that likely represent an overinterpretation of the available data.

Moho offsets and Moho gaps in the seismic interface play key roles in tectonic interpretations of 3-D crustal structure. When interpreted as a zone of absent Moho interface (Pfiffner *et al.* 1990), a gap in seismic information about the European Moho could be interpreted as a zone of symmetric subduction of lithosphere, a so-called 'Verschluckungs' zone (Laubscher 1970). It was shown for the Alpine region, however, that observed data gaps along near-vertical reflection profiles (Pfiffner *et al.* 1990) are not caused by an absent Moho interface. Holliger & Kissling (1992) imaged the expected Moho structure using wide-angle data from cross-profiles, and Valasek *et al.* (1991) imaged the Moho in the same region using wide-angle reflections along the EGT profile (see Fig. 14). These results obtained along the EGT transect by networked wide-angle and near-vertical profiling and the clear evidence for Moho offsets (see Figs 8 and 13), which indicate asymmetric subduction geometries with no need of Moho gaps, underline the

fact that the Moho interface exists everywhere below the Alps. Accordingly, the striving for highest continuity within carefully determined areas as a criterion for interface simplicity is justified.

In the Alpine region, Moho offsets are directly observed at only two locations below the EGT profile. The introduction of the least number of interfaces with the shortest lengths of offsets that fit all seismic data within their error limits is based on the principle of simplicity. In addition to clear Moho reflections from largely different depths within relatively short lateral distance, clear evidence for a Moho offset demands the *a priori* definition of error estimates for CSS data and 3-D migration. With respect to Moho topography in most areas, our proposed weighting scheme for CSS data to obtain error estimates might seem overly detailed. To test the evidence for a Moho offset, however, we feel that all terms of the weighting scheme are necessary. For geometrical reasons and as a result of the limited number of profiles, Moho offsets are only locally imaged by CSS data. Hence, modelling the lateral extent of such a Moho offset by connecting clusters of significant depth misfits (see Fig. 8 and Step 4 in the interface modelling procedure) relies strongly on plate-tectonic and geodynamic concepts and introduces additional ambiguity to the model.

The applied weighting scheme and the derived depth error estimates for seismic data are parameters that significantly influence the 3-D interface modelling results. We are well aware that the weighting scheme is still subjective, although we strove for as much objectivity as possible. As shown earlier in this study, altering the weighting scheme and consequently the depth error estimates does influence the roughness of the
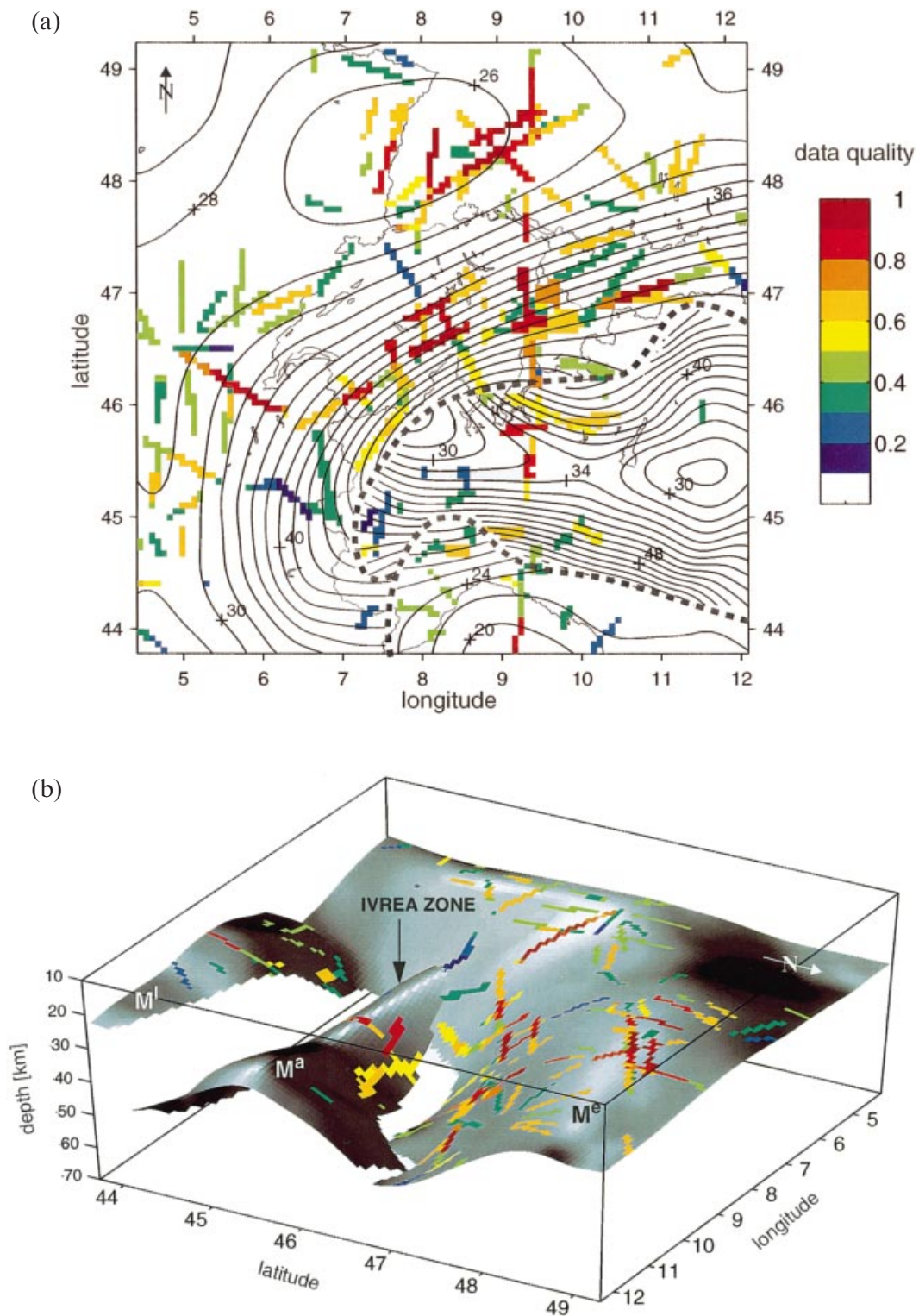
(a)

(b)

Figure 13. (a) Alpine Moho interface contoured at 2-km intervals derived by smoothest interpolation of the 3-D-migrated CSS data. Isoline values are indicated by numbers. The structural, 3-D-migrated database is shown by colours indicating weighting factors between 0.1 (information poorly constraint by CSS methods) and 1 (highly reliable reflectors from CSS methods) and by size of Fresnel zone on Moho interface. (b) Perspective SW view on the Moho below the Alpine region—European (M^e), Adriatic (M^a) and Ligurian (M^l) Moho.

resulting interfaces but it does not lead to significantly different interface offsets (see Fig. 9).

The new method to derive a seismic interface topography outlined in this study and applied to the Alpine Moho data quantitatively constrains the large-scale Alpine crustal structure (Fig. 13). The technique may be applied to Moho interfaces in other regions with sufficiently dense CSS data and to other interfaces (e.g. upper/lower crust discontinuity). Such
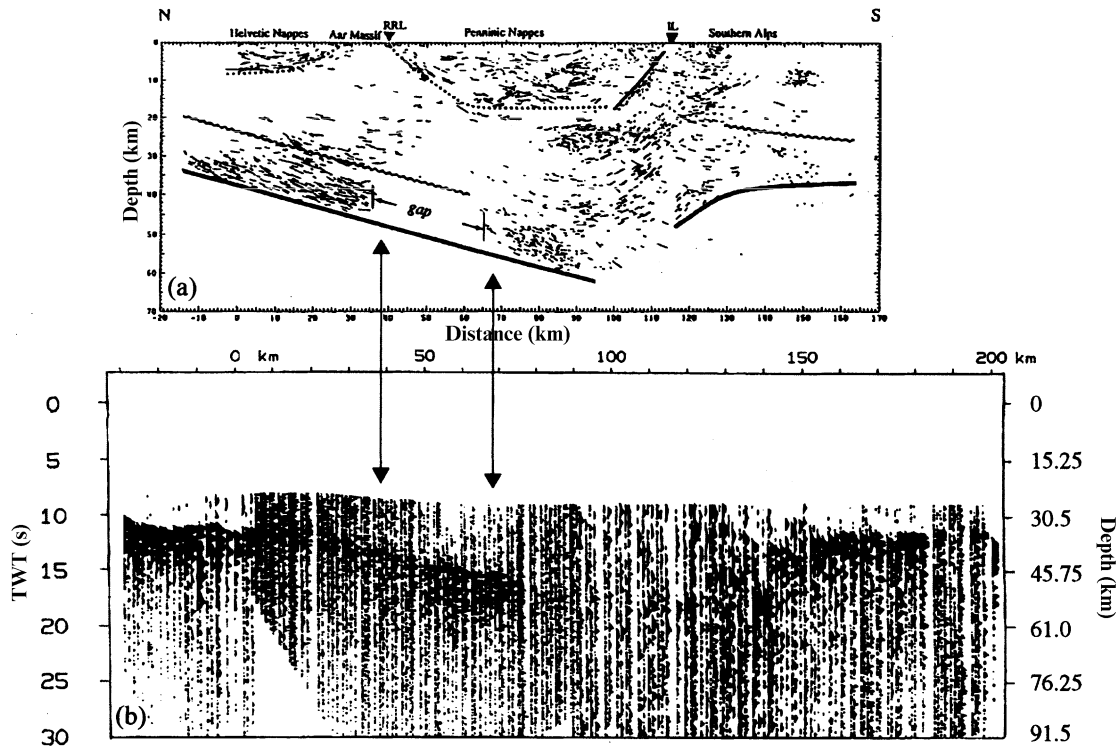
Figure 14. Summary of seismically determined 2-D main crustal structure and Moho depth along the NFP20 eastern transect (reproduced from Schmid *et al.* 1996). Horizontal and vertical scales are the same in both panels. (a) Migrated near-vertical reflections along the eastern traverse and generalized seismic crustal structure derived from orogen-parallel refraction profiles (Holliger & Kissling 1992). Solid lines indicate the position of the Moho, derived from orogen-parallel refraction profiles. (b) Normal-incidence representation of the wide-angle Moho reflections along the EGT refraction profiles perpendicular to the orogen (Valasek *et al.* 1991). Note that the gap in the reflectivity signal from the lower crust between 35 and 65 km profile distance in (a) is clearly covered by wide-angle reflection data.

consistently parametrized interface models are reproducible, updatable and regionally extendable. Besides serving as a base for tectonic interpretation, they are well suited for their use in computational processes. By integration into a 3-D velocity model, the Alpine Moho model has been successfully used for simulations of 3-D teleseismic wavefront distortion in the Alpine region (Waldhauser 1996), and it may also be used for gravity modelling by integration in a 3-D density model. Furthermore, the possibility of quantitative assessment of the reliability of a seismic model helps in designing future experiments aimed at improving and extending the present knowledge about the Alpine crust–mantle boundary.

ACKNOWLEDGMENTS

REFERENCES

Aichroth, B., Prodehl, C. & Thybo, H., 1992. Crustal structure along the Central Segment of the EGT from seismic-refraction studies, *Tectonophysics,* **207,** 43–64.

Ansorge, J., 1968. Die Struktur der Erdkruste an der Westflanke der Zone von Ivrea, *Schweiz. Mineral. Petrogr. Mitt.,* **48,** 247–254.

Ansorge, J. & Baumann, M., 1997. Acquisition of seismic refraction data within NFP20 (Switzerland), in *Deep Structure of the Swiss Alps: Results of NRP20,* pp. 25–30, eds Pfiffner, O.A., Lehner, P., Heitzmann, P., Mueller, St. & Steck, A., Birkhäuser Verlag, Basel.

Ansorge, J., Kissling, E., Deichmann, N., Schwendener, H., Klingelé, E. & Mueller, St., 1987. Krustenmächtigkeit in der Schweiz aus Refraktionsseismik und Gravimetrie, Abstract, Nat. Forschungsprogramm 20 (NFP20) 'Geologische Tiefenstruktur der Schweiz', Bull. **4,** 12.

Baumann, M., 1994. Three-dimensional modeling of the crust–mantle boundary in the Alpine region, *PhD thesis,* No. 10772, ETH-Zürich.

Berckhemer, H., 1968. Topographie des 'Ivrea–Körpers' abgeleitet aus seismischen und gravimetrischen Daten, German Research Group for Explosion Seismology, *Schweiz. Mineral. Petrogr. Mitt.,* **48,** 235–246.

Braile, L.W. & Chiang, C.S., 1986. The continental Mohorovicic discontinuity: results from near-vertical and wide-angle seismic reflection studies, in *Reflection Seismology: A Global Perspective,* pp. 257–272, eds Barazangi, M. & Brown, L., Geodynamics Series, **13,** Am. Geophys. Union, Washington, DC.

Buness, H., 1992. Krustale Kollisionsstrukturen an den Rändern der nordwestlichen Adriaplatte, Berliner Geowissenschaftliche Abhandlungen, **18,** Reihe B, FU Berlin.

Carrozzo, M.T., Luzio, D., Margiotta, C. & Quarta, T., 1991. Gravity map of Italy, in *Structural Model of Italy and Gravity Map,* ed. Scandone, P., quaderni de 'La Ricerca Scientifica' **114/3,** CNR, Rome.

Cline, A.K., 1974. Scalar and planar curve fitting using spline under tension, *Commun. ACM,* **17** (4), 218–220.

Colombi, B., Guerra, I. & Scarascia, S., 1977. Crustal structure along two seismic refraction lines in the Northern Apennines (lines 1b and 2), *Boll. Geof. Teor. Appl.,* **19** (75–76), 214–224.

Egger, A., 1992. Lithospheric structure along a transect from the Northern Apennines to Tunisia derived from seismic refraction data, *PhD thesis,* No. 9675, ETH-Zürich.

Egloff, R., 1979. Sprengseismische Untersuchungen der Erdkruste in der Schweiz, *PhD thesis,* No. 6502, ETH Zürich.

Freeman, R. & Mueller, St. (eds), 1992. Atlas of compiled data, in *A continent revealed: The European Geotraverse,* eds Blundell, D., Freeman, R. & Mueller, St., Cambridge University Press, Cambridge.

Giese, P. & Buness, H., 1992. Moho depth, in Atlas of compiled data, pp. 11–13, eds Freeman, R. & Mueller, St., in *A continent revealed: The European Geotraverse,* eds Blundell, D., Freeman, R. & Mueller, St., Cambridge University Press, Cambridge.

Giese, P., Prodehl, C. & Stein, A. (eds), 1976. *Explosion Seismology in Central Europe,* Springer-Verlag, Berlin.

Hitz, L., 1995. The 3D crustal structure of the Alps of eastern Switzerland and western Austria interpreted from a network of deep-seismic profiles, *Tectonophysics,* **248,** 71–96.

Holliger, K. & Kissling, E., 1991. Ray-theoretical depth migration: methodology and application to deep seismic reflection data across the eastern and southern Swiss Alps, *Eclogae Geol. Helv.,* **84/2,** 369–402.

Holliger, K. & Kissling, E., 1992. Gravity interpretation of a unified 2D acoustic image of the central Alpine collision zone, *Geophys. J. Int.,* **111,** 213–225.

Kissling, E., 1993. Deep structure of the Alps—what do we really know? *Phys. Earth planet. Inter.,* **79,** 87–112.

Kissling, E., Ansorge, J. & Baumann, M., 1997. Methodological considerations of 3-D crustal structure modeling by 2-D seismic methods, in *Deep Structure of the Swiss Alps: Results of NRP20,* pp. 31–38, eds Pfiffner, O.A., Lehner, P., Heitzmann, P., Mueller, St. & Steck, A., Birkhäuser Verlag, Basel.

Klingelé, E., 1972. Contribution à l'étude gravimétrique de la Suisse Romande et des régions avoisinantes, *Matériaux pour la Géologie de la Suisse,* Série Géophysique, **15,** Kümmerly & Frey, Geographischer Verlag, Bern.

Lancaster, P. & Salkauskas, K., 1986. *Curve and Surface Fitting,* Academic Press, New York.

Laubscher, H.P., 1970. Bewegung und Wärme in der Alpinen Orogenese, *Schweiz. Mineral. Petrogr. Mitt.,* **50,** 565–596.

Laubscher, H.P., 1983. The late Alpine (Periadriatic) intrusions and the Insubric Line, *Mem. Soc. Geol. It.,* **26,** 21–30.

Mayrand, L.J., Green, A.G. & Milkereit, B., 1987. A quantitative approach to bedrock velocity resolution and precision: the LITHOPROBE Vancouver Island experiment, *J. geophys. Res.,* **92,** 4837–4845.

Meissner, R. & Bortfeld, R.K. (eds), 1990. *Dekorp-Atlas,* Springer-Verlag, Berlin.

Meissner, R. and the DEKORP Research Group, 1991. The DEKORP survey: major achievements for tectonical and reflective styles, in *Continental Lithosphere: Deep Seismic Reflections,* pp. 69–76, eds Meissner, R., Brown, L., Dürbaum, H.J., Franke, W., Fuchs, K. & Seifert, F., Geodynamics Series, **22,** Am. Geophys. Union, Washington, DC.

Ménard, G., Molnar, P. & Platt, J.P., 1991. Budget of crustal shortening and subduction of continental crust in the Alps, *Tectonics,* **10/2,** 231–244.

Montrasio, A. & Sciesa, E. (eds), 1994. *Proceedings of Symposium 'CROP—Alpi Centrali',* Sondrio, 20–22 October 1993, Quad. Geodynamica Alpina e Quat., Milano.

Musacchio, G., De Franco, R., Cassinis, R. & Gosso, G., 1993. Reinterpretation of a wide-angle reflection 'fan' across the Central Alps, *J. appl. Geophys.,* **30,** 43–53.

Nadir, S., 1988. Structure de la croûte continentale entre les Alpes Occidentales et les Alpes Ligures et ondes S dans la croûte continental à l'ouest du Bassin de Paris, *PhD thesis,* University of Paris VII.

Parolai, S., Spallarossa, D. & Eva, C., 1997. Lateral variations of P_n wave velocity in northwestern Italy, *J. geophys. Res.,* **102** (B4), 8369–8379.

Pfiffner, O.A., Frei, W., Valasek, P., Stäuble, M., Levato, L., DuBois, L., Schmid, S.M. & Smithson, S.B., 1990. Crustal shortening in the Alpine orogen: results from deep seismic reflection profiling in the eastern Swiss Alps, line NFP20-east, *Tectonics,* **9/6,** 1327–1355.

Pfiffner, O.A., Lehner, P., Heitzmann, P., Mueller, St. & Steck, A. (eds), 1997. *Deep Structure of the Swiss Alps: Results of NRP20,* Birkhäuser Verlag, Basel.

Prodehl, C., Mueller, St. & Haak, V., 1995. The European Cenozoic rift system, in *Continental Rifts: Evolution, Structure, Tectonics,* pp. 133–212, ed. Olson, K.H., Elsevier, Amsterdam.

Roure, F., Heitzmann, P. & Polino, R. (eds), 1990. *Deep Structure of the Alps,* Vol. spec. Mem. Soc. geol. France, Paris, **156;** Mem. Soc. geol. Suisse, Zürich, **1;** Soc. geol. Italia, Rome, **1.**

Scarascia, S. & Cassinis, R., 1997. Crustal structures in the central-eastern Alpine sector: a revision of the available DSS data, *Tectonophysics,* **271,** 157–188.

Schmid, S.M., Zingg, A. & Handy, M., 1987. The kinematics of movements along the Insubric Line and the emplacement of the Ivrea Zone, *Tectonophysics,* **135,** 47–66.

Schmid, S.M., Pfiffner, O.A., Froitzheim, N., Schönborn, G. & Kissling, E., 1996. Geophysical–geological transect and tectonic evolution of the Swiss–Italian Alps, *Tectonics,* **15/5,** 1036–1064.

Sénéchal, G. & Thouvenot, F., 1991. Geometrical migration of line-drawings: a simplified method applied to ECORS data, in *Continental Lithosphere: Deep Seismic Reflections,* pp. 401–407, eds Meissner, R., Brown, L., Dürbaum, H.J., Franke, W., Fuchs, K. & Seifert, F., Geodynamics Series, **22,** Am. Geophys. Union, Washington, DC.

Slejko, D., *et al.,* 1987. *Modello Sismotettonico dell'Italia Nord-Orientale,* Consiglio Nazionale delle Ricerche, Gruppo Nazionale per la Difesa dai Terremoti, Rendiconto no. **1,** Trieste, Italy.

Solarino, S., Kissling, E., Sellami, S., Smriglio, G., Thouvenot, F., Granet, M., Bonjer, K.P. & Sleijko, D., 1997. Compilation of a recent seismicity data base of the greater Alpine region from several seismological networks and preliminary 3D tomographic results, *Ann. Geofis.,* **XL, 1,** 161–174.

Spakman, W., Van der Lee, S. & Van der Hilst, R., 1993. Travel-time tomography of the European–Mediterranean mantle down to 1400 km, *Phys. Earth planet. Inter.,* **79,** 3–74.

Stein, A., Vecchia, O. & Froelich, R., 1978. A seismic model of a refraction profile across the western Po valley, in *Alps, Appenines, Hellenides,* pp. 180–189, eds Closs, H., Roeder, D. & Schmidt, K., Schweizerbart Verlag, Stuttgart.

Thouvenot, F., Paul, A., Sénéchal, G., Hirn, A. & Nicolich, R., 1990. ECORS–CROP wide-angle reflection seismics: constraints on deep interfaces beneath the Alps, in *Deep Structure of the Alps,* pp. 97–106, eds Roure, F., Heitzmann, P. & Polino, R., Vol. spec. Mem. Soc. geol. France, Paris, **156;** Mem. Soc. geol. Suisse, Zürich, **1;** Soc. geol. Italia, Rome, **1.**

Valasek, P., 1992. The tectonic structure of the Swiss Alpine crust interpreted from a 2D network of deep crustal seismic profiles and an evaluation of 3D effects, *PhD thesis,* No. 9637, ETH-Zürich.

Valasek, P. & Mueller, St., 1997. A 3D tectonic model of the central Alps based on an integrated interpretation of seismic refraction and NRP20 reflection data, in *Deep Structure of the Swiss Alps: Results of NRP20,* pp. 305–325, eds Pfiffner, O.A., Lehner, P., Heitzmann, P., Mueller, St. & Steck, A., Birkhäuser Verlag, Basel.

Valasek, P., Mueller, St., Frei, W. & Holliger, K., 1991. Results of NFP 20 seismic reflection profiling along the Alpine section of the European Geotraverse (EGT), *Geophys. J. Int.,* **105,** 85–102.

Waldhauser, F., 1996. A parametrized three-dimensional Alpine crustal model and its application to teleseismic wavefront scattering, *PhD thesis,* No. 11940, ETH-Zürich.

Waldhauser, F., Kissling, E., Baumann, M. & Ansorge, J., 1994. 3D seismic model of the crust under the central and western Alps (Abstract), European Geophysical Society, XIX General Assembly, Grenoble, *Ann. Geophys.,* **12,** Suppl. I, C23.

Ye, S., Ansorge, J., Kissling, E. & Mueller, St., 1995. Crustal structure beneath the eastern Swiss Alps derived from seismic refraction data, *Tectonophysics,* **242,** 109–221.